

Search for X-ray occultations in Active Galactic Nuclei

G. Torricelli-Ciamponi^{1*}, P. Pietrini², G. Risaliti^{1,3}, M. Salvati¹

¹ *INAF - Osservatorio Astrofisico di Arcetri, L.go E. Fermi 5, Firenze, Italy*

² *Università di Firenze, Largo E. Fermi 2, Firenze, Italy*

³ *Harvard-Smithsonian Center for Astrophysics, 60 Garden St. Cambridge, MA 02138 USA E-mail: grisaliti@cfa.harvard.edu*

Released Xxxx Xxxxx XX

ABSTRACT

Recent time-resolved spectral studies of a few Active Galactic Nuclei in hard X-rays revealed occultations of the X-ray primary source probably by Broad Line Region (BLR) clouds. An important open question on the structure of the circumnuclear medium of AGN is whether this phenomenon is common, i.e. whether a significant fraction of the X-ray absorption in AGN is due to BLR clouds. Here we present the first attempt to perform this kind of analysis in a homogeneous way, on a statistically representative sample of AGN, consisting of the ~ 40 brightest sources with long *XMM-Newton* and/or *Suzaku* observations. We describe our method, based on a simple analysis of hardness-ratio light curves, and its validation through a complete spectroscopic analysis of a few cases. We find that X-ray eclipses, most probably due to clouds at the distance of the BLR, are common in sources where the expected occultation time is compatible with the observation time, while they are not found in sources with longer estimated occultation times. Overall, our results show that occultations by BLR clouds may be responsible for most of the observed X-ray spectral variability at energies higher than 2 keV, on time scales longer than a few ks.

Key words: galaxies: active– galaxies: Seyfert– X-rays: galaxies

1 INTRODUCTION

A circumnuclear, toroidal absorber is a key element in the structure of Active Galactic Nuclei (AGN), as implied by AGN Unified Models (Antonucci 1993, Urry & Padovani 1995), and confirmed by a large set of observational data (e.g. Bianchi, Maiolino, Risaliti 2012 for a recent review). The composition, geometry and inner structure of this absorber has been long investigated, with evidence of a large spread of properties and dimensions, ranging from sub-pc to hundreds pc scales, and from largely homogeneous to clumpy structures. In this context, a key piece of information comes from measurements of X-ray absorption column densities (N_H): in almost all sources with multiple hard X-ray observations, the values of N_H show high variability (Risaliti et al. 2002). This result implies a clumpy structure of the circumnuclear absorber, and an upper limit on its distance from the central source ranging from a fraction to several tens of parsecs, depending on the time separation between the observations (and assuming Keplerian velocities for the obscuring clouds). In order to refine these measurements, it is necessary to investigate absorption variability at shorter time scales, with the aim of reducing the upper limits on the

variation times (through campaigns of multiple observations of the same sources), or to directly measure them (if the N_H changes occur during single long observations).

Several such studies have been performed in the past few years, on a small number of sources: NGC 3227 (Lamer, Uttley & McHardy 2003), NGC 1365 (Risaliti et al. 2007, 2009; Maiolino et al. 2010), NGC 4388 (Elvis et al. 2004), Mrk 766 (Risaliti et al. 2011), NGC 4151 (Puccetti et al. 2007), NGC 7582 (Bianchi et al. 2009; Piconcelli et al. 2007), UGC 4203 (Risaliti et al. 2010), NGC 4395 (Nardini & Risaliti 2011); SWIFT J2127.4+5654 (Sanfrutos et al. 2013). A review of several of these observations is presented in Risaliti (2010).

Most of these studies were performed following a two-step strategy:

- 1) When a flux light curve shows strong variability and such strong variations are also observed in the corresponding hardness ratio light curve, a change in the spectral shape must be present. It is possible to interpret the observed spectral variations in two different ways: *i*) as due to changes in absorption properties, such as N_H and covering factor, of clouds crossing the line of sight towards the X-ray source; *ii*) as due to changes of the slope of the intrinsic continuum.

- 2) A complete spectral analysis is performed on each time interval defined in the first step, in order to deter-

* E-mail: torricel@arcetri.astro.it

mine whether the observed variability can be explained by a change in the photon spectral index. In all the cases mentioned above, this analysis confirmed that the spectral variations were due to changes in the absorbing column density, occurring on time scales from a few hours to a few days.

The physical consequences of these results are quite relevant in the context of AGN structure and physics. Assuming that the observed occultations are due to clouds orbiting the central black hole/X-ray source with Keplerian velocity, the main conclusions of the studies performed so far are the following:

- The X-ray “torus” is made of cloud-like structures with the same density and distance from the center as those of the broad line region (BLR) emission line clouds (Bianchi, Maiolino & Risaliti 2012). Therefore, in at least some sources, the X-ray absorber and the Broad Line region are one and the same (Maiolino et al. 2010).
- The short transit time of these clouds across the X-ray sources, compared with the estimated black hole masses, is a direct observational proof that the X-ray source has a size of a few gravitational radii, as commonly assumed in disk+corona models (see for example Haardt & Maraschi 1993).
- In a few cases with high S/N observations, we were able to investigate the structure of the obscuring clouds, inferring a “cometary” shape (Maiolino et al. 2010; Risaliti et al. 2011).
- If X-ray occultations occur during an observation, they must be considered in the spectral analysis, even when the purpose of the study is not related to absorption-related issues. Alternatively, a wrong estimate of the other spectral parameters is possible, as demonstrated in the case of NGC 4395 (Nardini & Risaliti 2011).

All these results have been obtained through a large observational and analytical effort on a small number of “ad-hoc” sources. The clearest example in this sense is NGC 1365, which is one of the most monitored AGNs, with several observations with each of all the main X-ray observatories in the past few years, only because of its known high frequency of occultation events.

It is therefore fundamental to move from a “one by one” analysis to a more general study of a statistically significant sample of AGN, in order (a) to estimate how common are X-ray occultations, and (b) whether the properties of the X-ray source and of the absorbing clouds inferred from previous studies are typical of AGNs.

This ambitious task requires the availability of a huge amount of high-quality X-ray data, which can be obtained only through archival observations, and a similarly large analysis work, which is probably beyond the capabilities of any single group. However, we believe we can obtain significant results with a simplified approach, based on a refined analysis of hardness ratio light curves (the first step in the strategy summarized above) and avoiding a complete time-resolved spectral analysis. In this paper we present this new method, and the main results from a statistical analysis of its application to a large, well defined sample. We will demonstrate that a careful time analysis can effectively discover occultations with durations of the same length, or shorter, than the observing time, and with column densities in the range 10^{23} - 10^{24} cm⁻². We will also show that these events are quite common among AGNs, implying that broad line

clouds are in many cases the source of the observed X-ray absorption.

In Section 2 we define a sample of ~ 40 X-ray bright AGNs with long X-ray observations, with suitable archival X-ray observations. In Section 3 we outline the method, which is based, and calibrated, on our past works on time-resolved spectroscopy of selected sources. In Section 4 we discuss the results, focusing on testing the ability of our analysis to discriminate between actual occultations and other possible variability causes. In Section 5 we discuss the physical implications of our results, especially regarding the statistics of the occurrence of the occultations. Our conclusions are presented in Section 6, while a complete discussion of all the physical consequences of our results will be presented in a forthcoming, companion paper (Pietrini et al. 2014, in preparation).

2 OBSERVATIONS: THE SAMPLE

Our aim is to analyze a representative, unbiased sample of local AGN. Our main requirements are the following.

- 1) A high X-ray flux, in order to detect possible spectral changes due to occultations with high statistical significance. In principle, our search may be extended to the whole X-ray domain, however, due to additional spectral complexities below 2 keV (soft excess, diffuse emission, warm absorbers), and to poor signal-to-noise above 10 keV, we will restrict our analysis in the 2-10 keV range. This implies that our search will be sensitive only to occultations by clouds with column density in the range 10^{23} - 10^{24} cm⁻² and that our sensitivity in disentangling spectral index variations and absorption variations is limited. We will further discuss this limitation in the next Sections.

- 2) A “long enough” exposure time. The definition of a minimum acceptable duration is not straightforward, because both physical and technical considerations may be relevant. Operationally, we may define a minimum duration based on the source flux: the higher the flux, the shorter the time needed to identify an occultation through spectral analysis. From a physical point of view, we may expect that the typical duration of an occultation depends on the size of the X-ray source and, therefore, on the black hole mass. Since we do not want to introduce biases based on our physical expectations, we did not consider the latter criterion in the composition of the sample; however its impact is discussed in detail in Section 5.

- 3) High-sensitivity instruments, in order to obtain the highest possible count rate for each source.

Based on the above requirements, we composed a sample of bright AGNs, consisting of all sources with 2-10 keV flux higher than 2×10^{-11} erg s⁻¹ cm⁻², where the X-ray flux was estimated extrapolating the measured 15-195 keV flux from the *Swift*/BAT 54 month catalogue (Cusumano et al. 2010). This choice is based on the completeness of such AGN sample in terms of *intrinsic* X-ray flux: absorption with column densities below $\sim 10^{24}$ cm⁻² does not affect the observed flux in the 14-195 keV energy band (this is not the case for thicker absorbers: for this reason Compton-thick sources were excluded from our study, see below). In order to study the effects of absorption variability, we need bright sources in term of intrinsic, rather than observed, flux (i.e.

in order to measure N_H variations with small errors we need a high S/N at energies *above* the photoelectric cut off). For this reason, the Swift/BAT sample is preferred over other samples directly selected in the 2-10 keV band, such as the Piccinotti et al. (1982) sample. Among these sources, we selected those with available observations made before January 2012, by *XMM-Newton* and/or *Suzaku*, with durations of at least 80 ks and 50 ks, respectively. The reason for a different choice of the observation duration for the two different instruments is the fact that the resulting useful time interval is different in the two cases (see the end of Section 3.1 for an explanation).

Starting from this initial catalog, we made some "ad-hoc" corrections: (1) we excluded sources known to be reflection-dominated in the 2-10 keV range (such as NGC 4945, Mrk 3 or Circinus) and other sources for which *XMM* data are dominated by background flares or with calibration problems among the various XIS instruments for *Suzaku* observations (Centaurus A, QSO B0241+62, Mrk 6); (2) we included NGC 4395 which, though slightly fainter than our flux limit, has been extensively searched for occultations (Nardini & Risaliti 2011) and can be a useful comparison/calibration source for our analysis.

The choice of the instruments and of the observations duration is based on our past experience with single sources, and on the requirement of a final sample with a large enough size (42 sources, 85 observations) for a detailed statistical study, but still manageable for individual studies of each individual observation.

The final sample is clearly not complete, but we believe it is truly representative of the AGN population, because all the adopted selection criteria are not related to the possible presence of occultations or, more in general, to the variability behaviour of these sources. The only possible exception may be the case of NGC 1365, which is over-represented in the sample, because the large number of available observations is primarily due to the high frequency of detected X-ray occultations.

Moreover, several interesting cases remain out of our sample, such as the occultation studies based on campaigns of repeated short observation (e.g., UGC 4203, Risaliti et al. 2010), the extreme N_H changes revealed by TOO observations triggered by long-term monitoring (e.g. NGC 4388, Elvis et al. 2004), and the long monitoring of the brightest sources made with lower effective area instruments (such as the eclipse discovered in a BeppoSAX observation of NGC 4151, Puccetti et al. 2007). These cases can be discussed one-by-one, but are not included in our sample, to preserve its homogeneity.

The main properties of the sample, consisting of 32 *XMM-Newton* observations and 53 *Suzaku* observations of a total of 42 sources, are presented in Table 1. It is apparent from Table 1 that our sample includes a wide range in source brightness and in central black hole masses as well as all possible choices of source type ranging from "pure" Seyfert 1 to Seyfert 2.

3 OUR ANALYSIS

3.1 Data reduction

The data have been reduced and analyzed following a standard procedure, which we already described in other similar works (e.g. Risaliti et al. 2009 for *XMM-Newton* data and Maiolino et al. 2010 for *Suzaku* data).

For *XMM-Newton*, the light curves were extracted from the PN cleaned event files in the circular region including most of the emission. For the bright sources of our sample this radius results ~ 37 arcsec. The background was extracted from a nearby region free of detectable sources. The high X-ray flux of our sources implies that the background counts are in all cases negligible, and our analysis does not depend on the particular choice of the background region. The high source brightness is also the reason of the relatively large source extraction area: we find that such a radius optimizes the signal-to-noise in our light curves, by including the tails of the point spread function up to a $\sim 99\%$ encircled effective area.

For *XMM-Newton* data, the only non-completely straightforward aspect of the reduction is the choice of the rejection level for the high-energy background flares. We have chosen a somewhat different approach depending on the observation mode. For observations in "small window" mode, since our sources are bright, we have generally adopted a threshold only slightly higher than the conservative level suggested in the *XMM-Newton* data reduction guide for EPIC instrument, namely 1count/s. In the cases of "full window" observations, we have chosen to allow for a relatively higher level, depending on the observation, with the aim of rejecting only the time intervals in which the background flares appear to saturate the instruments. In the subsequent analysis of the resulting light curves, we have checked that no apparently significant hardness ratio variation features were present right in those time intervals that a more conservative choice of the threshold would have rejected. The selection of the appropriate time intervals has been done analysing the counts/s light curves in the 10-13 keV energy band, since in this range, due to the strong cut-off in *XMM* effective area at ~ 10 keV, a negligible contribution to the counts/s is expected from the source and most of the detected photons originate from background proton flare events.

For *Suzaku* data, light curves were obtained from a 2 arcmin circular region. The background was extracted from clean regions in the same frames. All the available XIS spectra have been used for each observation when the data were compatible.

Since our analysis is based on hardness ratio light curves, we need to have a relatively high number of counts in each time bin. For this reason, the light curves were generally grouped in 2000 s both for *XMM-Newton* and *Suzaku* data.

The hardness ratio (*HR*) light curves have been obtained from the ratio of the hard and soft curves. The exact energy range of these two curves is 2-4 keV and 5-10 keV, and has been carefully selected based on the procedure described below. The error in the ratio has been estimated by applying a standard error propagation, assuming independent factors. This may lead in some cases to an over-estimate of the actual uncertainties in the hardness ratio light curve,

Table 1. The sample of bright AGN with long, high S/N X-ray observations. (1): log of black hole mass in unit of M_{\odot} ; (2): eclipsing time (10^3 s) computed as described in Sect.5, (3): 2-10 keV flux (10^{-11} erg/cm²/s), obtained extrapolating the *Swift*/BAT observed spectrum. (4): Number of *XMM-Newton* and *Suzaku* observations considered in the analysis (more details on the single observations are presented in Table 2).

Name	redshift	Type	M_{BH} (1)	t_{ecl} (2)	F(2-10) (3)	<i>XMM</i> (4)	<i>Suzaku</i> (4)	References ^a
NGC 4151	0.0033	1.5	7.66	120	22.86	0	2	18,19
IC 4329A	0.0160	1	8.3	1565	18.32	1	0	2
NGC 5506	0.0062	1.9	6.7	112	16.70	1	2	20
MCG 5-23-16	0.0085	2	7.7	428	14.73	1	1	3
NGC 4388	0.0084	2	6.92	152	11.58	0	1	14
NGC 2110	0.0078	2	8.3	678	11.31	0	1	4,5
NGC 4507	0.0118	2	8.4	1096	10.63	0	1	3
NGC 3783	0.0097	1.5	7.5	132	10.41	2	2	1
NGC 3227	0.0039	1.5	6.9	55	7.06	1	1	13
MCG 08-11-011	0.0205	1.5	8.1	1033	6.87	0	1	4,5,6
NGC 3516	0.0088	1.2	7.5	147	6.76	1	2	13
MCG 06-30-015	0.0078	1.2	6.3	63	6.69	2	3	2
3C 111	0.0485	1	9.6	11109	6.64	1	4	7
MCG 02-58-022	0.0469	1.5	8.4	2727	6.44	0	1	8
1H 2251-179	0.0640	1	8.8	5448	6.03	0	1	3
Mrk 509	0.0344	1.2	8.2	779	5.49	1	1	1,5
3C 120	0.0330	1	7.8	457	4.97	1	2	15
3C 382	0.0579	1	9.2	7079	4.54	0	1	3,4
IGR J21277+5656	0.0147	NLS1	7.18	239	4.44	1	1	11,12
Mrk 110	0.0353	NLS1	7.4	227	4.14	0	1	1
NGC 4593	0.0090	1	7.0	90	4.10	0	1	9
NGC 7469	0.0163	1.2	7.1	155	4.06	2	1	1
Ark 120	0.0327	1	8.2	685	4.05	0	1	1
NGC 7582	0.0052	2	8.3	351	3.90	1	0	3
NGC 1142	0.0288	2	9.4	4552	3.84	0	1	3
NGC 4051	0.0023	1.5	6.2	21	3.75	0	3	13
MCG 3-34-64	0.0165	2	8.3	915	3.60	1	0	3
4U 0106-59	0.0470	1.2	8.4	862	3.50	1	2	1
NGC 1365	0.0055	1.8	6.3	34	3.36	2	3	16
Mrk 79	0.0222	1.2	7.7	317	3.36	1	1	1
ESO 141-55	0.0366	1.2	7.1	377	3.10	1	0	10
3C 445	0.0564	1.5	8.3	2119	3.10	0	1	7
EXO 055620-3820,2	0.0340	1.2	8.4	1622	3.07	1	0	3
NGC 7314	0.0048	1	6.0	21	2.99	0	1	5
NGC 5548	0.0172	1.5	7.6	239	2.92	1	0	13
PG 1501+106	0.0364	1.5	8.15	503	2.63	0	4	3,4
Mrk 766	0.0129	NLS1	6.5	83	2.61	6	2	6
Mrk 279	0.0305	1	7.5	258	2.56	0	1	1
RHS 39	0.0222	1	8.7	1368	2.33	1	0	3,6
2MASX J04532576+0403416	0.0296	2			2.15	0	1	
NGC 1052	0.0050	2	8.2	240	2.10	0	1	6
NGC 4395	0.0011	1.5	5.56	2.6	1.16	1	0	17

^a (1) Peterson et al. (2004), (2) Zhou et al. (2010), (3) Winter et al. (2009), (4) Winter et al. (2010), (5) Middleton, Done & Schurch (2008), (6) Beckmann et al. (2009), (7) Grandi, Malaguti & Fiacchi (2006), (8) Rivers, Markowitz & Rothschild (2011), (9) Denney et al. (2006), (10) Whang & Zhang (2007), (11) Malizia et al. (2008), (12) Miniutti et al. (2009), (13) Denney et al. (2010), (14) Kuo et al. (2011), (15) Grier et al. (2012), (16) Risaliti et al. (2009), (17) Peterson et al. (2005) (18) Onken et al. (2007), (19) Bentz et al. (2006), (20) Guainazzi et al. (2010).

because the fluctuations of the hard and soft energy intervals at a given time are not always completely independent. In order to quantify this effect, we analyzed the dispersion with respect to a constant average value of the light curves where no variability was detected (a subsample of ~ 15 unobscured sources). In almost all cases the reduced χ^2 is higher than 0.8, with two exceptions with values around 0.5. An F-test showed that these values are in most objects com-

patible with purely statistical errors, with a zero-hypothesis threshold of 5%. When the probability of purely statistical errors was lower than 5%, we estimated the average fraction by which we should decrease the measured errors in order to obtain a 5% probability. These fractions are negligible in all cases, except for the two objects mentioned above, where they are of the order of 20-25%. We conclude that the hardness ratio errors calculated assuming independent

errors in the two energy intervals are a good approximation of the true statistical errors. If in a few cases systematic effects added a small contribution to the errors, this would imply an under-estimate of the significance of possible HR variations, but not the inclusion of any spurious occultation event.

For each source, reduced and analysed data are indicated in Table 2 and identified by the observation date and by the observing instrument. The effective duration of the observation, Δt_{eff} (expressed in ks), is also indicated. By “effective” duration we imply the total time extent over which the light curve is actually reliable, that is excluding those intervals in which background “proton” flares may affect the resulting counts, as far as *XMM-Newton* light curves are concerned. On the other hand, for *Suzaku* observations, the time interval over which a source is actually observed is in general significantly longer than the reported exposure time (mainly because of Earth occultations), therefore our “effective” duration represents the total time interval over which we can analyze the light curve behavior.

3.2 Choice of the hardness ratio energy bands

The choice of the optimal energy intervals for the computation of the hardness ratio is not straightforward, because the measured counts in each energy band depend on the energy-dependent effective area. Therefore, we need to make the convolution of several different models (corresponding to several different absorbing conditions) with the instrumental response and thus calculate the expected counts/s, in order to identify which energy bands are most appropriate for our analysis, that is maximise the observable effects of absorbing column density differences. Obviously this choice also depends on which range of column density we are most interested in. In order to simplify our analysis, we decided to neglect all the information below 2 keV. In this way, we loose sensitivity to low-column density ($N_H < 10^{22} \text{ cm}^{-2}$) variations, but we also avoid the complications related to the possible presence of warm absorbers. In principle, this is not an absolutely needed simplification: complete spectral fits can easily distinguish between warm and neutral absorbers. However, this requires some extra effort in the interpretation of the light curves, and is left for future extensions of our work.

Within the 2-10 keV band, we have computed photon fluxes for different energy ranges, namely $F(2-4 \text{ keV})$, $F(3-5 \text{ keV})$, $F(5-10 \text{ keV})$, $F(6-10 \text{ keV})$, assuming an emitted spectrum consisting of an absorbed power-law model, with photon index γ , where N_H is the column density of the absorbing gas of the cloud crossing the line of sight and C_F is the intervening absorbing gas covering factor. We used the XSPEC package to calculate the expected counts/s in each energy range, convolving our models with the instrumental response matrices for both *XMM* EPIC and *Suzaku* XIS instruments, and to derive, from these “synthetic” fluxes, the expected hardness ratio. This procedure has been performed for different values of N_H and of the covering factor C_F due to the cloud passage, assuming $\gamma = 2$ as a representative value for the photon index. Four different hardness ratio combinations, namely $HR_1(N_H, C_F) = F(5-10 \text{ keV})/F(2-4 \text{ keV})$, $HR_2(N_H, C_F) = F(6-10 \text{ keV})/F(2-4 \text{ keV})$, $HR_3(N_H, C_F) = F(5-10 \text{ keV})/F(3-5 \text{ keV})$,

$HR_4(N_H, C_F) = F(6-10 \text{ keV})/F(3-5 \text{ keV})$, have been computed together with their respective errors, σ_i .

In order to quantify which one, among the hardness ratio combinations HR_i defined above, undergoes the largest variation owing to an obscuring cloud crossing the line of sight, we have compared each combination with the corresponding “unperturbed” hardness ratio, $HR_i(N_H = 0)$, evaluating the significance of the difference by means of the quantity

$$\Delta_i = \frac{HR_i(N_H, C_F) - HR_i(0, 0)}{[\sigma_i^2(N_H, C_F) + \sigma_i^2(0, 0)]^{1/2}}$$

defined for each combination ($i = 1, 2, 3, 4$) and for different values of N_H and covering factor C_F . We note that in our models we did not include the iron line since, for the column density values $N_H < 7 \times 10^{23} \text{ cm}^{-2}$ that we are dealing with, its contribution to the hard band counts is negligible. The comparison among the obtained Δ_i values for N_H in the range $1 \times 10^{23} < N_H < 7 \times 10^{23} \text{ cm}^{-2}$ shows that the Δ_i behaviour obviously depends on the choice of the soft energy range in the hardness ratio denominator. We obtain two different “groups” which differ essentially in their trend at low values of the optical depth, i.e. for $N_H < 3 \times 10^{23} \text{ cm}^{-2}$. Hardness ratios computed with the 2-4 keV energy band show larger Δ_i values with respect to those evaluated using the 3-5 keV band, owing to the energy position of the absorption cutoff. Within each “group” we have $\Delta_1 \gtrsim \Delta_2$ and $\Delta_3 \gtrsim \Delta_4$, indicating that the range 5-10 keV can be a better choice for the hard band. This result is due to the larger number of counts when the energy band 5-10 keV is used, due to the sharp decrease of the instrument effective area (of both *XMM* EPIC and *Suzaku* XIS) at energies higher than 6 keV. As a consequence, the choice $HR = F(5-10 \text{ keV})/F(2-4 \text{ keV})$ maximizes the hardness ratio variation for N_H values in the range $1 \times 10^{23} < N_H < 3 \times 10^{23} \text{ cm}^{-2}$; this result holds also for the case of a partial covering of the source ($C_F = 0.5$). Therefore, we conclude that the choice $HR \equiv HR_1$ is the most appropriate to our purposes. The same is true in the case of Seyfert 2 sources for which a constant absorption $N_H = 1 \times 10^{23} \text{ cm}^{-2}$ is assumed in addition to the variable cloud absorption.

3.3 A systematic search: our method of investigation

For each of the sources in our sample, we performed a quantitative analysis of the hardness ratio light curves, consisting of the following steps.

From the obtained HR light curves, it is apparent that there are sources for which the hardness ratio is largely constant in time, while for other sources there are time intervals, within the observation length, in which the HR value undergoes slight or significant variations. In order to point out and to quantify this variability the following procedure has been adopted. First of all, each HR light curve has been fitted with a constant, K_0 , and the value of the corresponding reduced “chi-square” $\chi^2/d.o.f. \equiv \chi_r^2$ has been computed; we refer to the reduced “chi-square” for the case of the initial fit with a constant only as $(\chi_r^2)_0/(d.o.f.)_0 \equiv \chi_{r0}^2$. The values of these three quantities $[\chi_{r0}^2, (d.o.f.)_0, K_0]$ are listed in Table 2. There are cases in which the χ_{r0}^2 value is close to

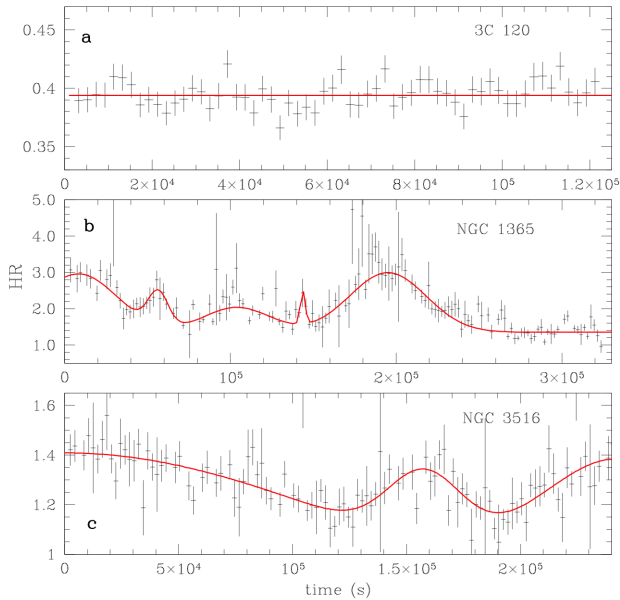


Figure 1. Three different examples of hardness ratio light curves and of the computed data fit (red continuous curves): a) the 08/26/03 *XMM-Newton* observation of 3C 120; b) the 01/21/08 *Suzaku* observation of NGC 1365; c) the 10/12/05 *Suzaku* observation of NGC 3516.

unity, thus ensuring that the fit with a constant value gives a good representation of the *HR* light curve. These are the cases in which no candidate eclipsing event can be identified from the observation and no further analysis is to be performed. As an example, the *XMM-Newton* observation of 3C 120 performed on 08/26/2003 is presented in Fig. 1a, where the hardness ratio light curve is shown, together with the fit with a constant [$(\chi^2)_0/58 = \chi^2_{r0} = 0.98$].

On the other hand, there are several cases for which the opposite conclusion holds. Although the true goodness of a fit depends *both* on the χ^2 value *and* on the number of degrees of freedom (*d.o.f.*), we *operationally* choose to define the value $(\chi^2)_0/(d.o.f.)_0 = 1.1$ to be the limit between the two classes of cases mentioned above, as a simple way to *conservatively* select observations deserving further study. For the cases with $\chi^2_{r0} > 1.1$ a better fit is sought for. In order to perform a new fit, we define a general form for more complex models for the *HR* light curve, described by the following functional form $G_N(t)$:

$$G_N(t) = K_N + \sum_{n=1}^N A_n e^{-\frac{1}{2} \left(\frac{t-t_n}{w_n} \right)^2}. \quad (1)$$

In the above expression we suppose to represent the trial function as a constant plus a number N of different gaussian components. For each n -th gaussian component, t_n defines the gaussian center, i.e. the time at which the *HR* reaches its local maximum value; A_n is the normalization of the n -th gaussian component and is positive definite, since an occultation is bound to produce an increase in the hardness ratio value above the constant level, K_N , and w_n is related to the width of the same n -th gaussian component.

Hence, for light curves such that the fit with a constant function (i.e., $N = 0$, $G_N(t) = G_0(t)$) results in $\chi^2_{r0} > 1.1$,

a new fit is performed using $G_1(t)$ with $N = 1$, that is testing a model composed of a constant plus one gaussian component, as a first step to improve the description of the light curve, and a new value of $\chi^2 = \chi^2_1$ is obtained. If this new fit is still not “satisfactory”, we proceed further on by adding another gaussian component to the model function ($G_2(t)$, $N = 2$) and re-fitting the light curve. This step-by-step procedure for improving the model descriptive capability by adding one gaussian component at a time should go on until a “satisfactory” fit is obtained with a model function $G_N(t)$ including a number N of gaussian components. The procedure leads to a meaningful result only if we define a quantitative measure for a fit to be more “satisfactory” than the previous, less complex, one. Therefore, in order to quantify the improvement of each new step fit with respect to the previous one and hence to estimate the significance of each newly added gaussian component, we have applied the F-test. The F-test calculates the null probability value, F_n , on whose basis one can reject the simpler model (as worse) and maintain the more complex one (as a better description of the data) or not. We accept the more complicated model as the best one if the F_n value is less than 0.05. Following this method, for each step of our procedure, we use the F-test to compare the fit with a function including n gaussian components plus a constant with the previous step (the “simpler” one), for which the describing model is defined by $(n - 1)$ gaussian components plus a constant. This way, the null probability value, F_n , that we obtain is indeed a measure of the significance of the additional n -th gaussian component. To exemplify, comparing the $G_0(t) = K_0$ model, representing the light curve with a simple constant, with the next fitting step, including one gaussian component and described by $G_1(t) = K_1 + A_1 e^{-\frac{1}{2} \left(\frac{t-t_1}{w_1} \right)^2}$, the null probability value F_1 gives the significance of the *HR* time variation that we attempt to describe with the gaussian component defined by the parameters $\{A_1, t_1, w_1\}$, given by the fit; the same will occur at each further step, allowing us to associate a significance estimate F_n to all the gaussian components $\{A_n, t_n, w_n\}$ (with $n = 1 \dots N$) that compose our final fit (attained when F_n becomes larger than 0.05).

An example of this case is presented in Fig. 1b where the hardness ratio of the 01/21/2008 *Suzaku* observation of NGC 1365 and the derived fit with 5 gaussian components are shown. As it is apparent, in this case *HR* is a variable function of time, but during the last third of the observation interval its value becomes almost constant. This fact is important, since the fit can easily determine the constant *HR* level to which the gaussian components induced by occultations add up.

The values of the quantities (A_n, F_n) , i.e. the peak value of the n -th gaussian component and its significance, are reported in Table 2 for those components having $F_n < 0.05$. As described before, we follow this procedure until F_n becomes greater than 0.05. However, as we shall discuss in the next Sections, we will choose a much more conservative significance threshold to identify the “safe” occultation events.

We note that our choice of gaussian functions is arbitrary, but quite effective. Since the shape of the *HR* light curves is not predictable, our aim was to reproduce the most significant variations with simple functions, defined just by some measure of height and width. A triangular function,

or similar shapes, would also be acceptable. However, the choice of the exact shape of the function does not affect our analysis and our results.

There are some cases in which the above procedure fails because the light curve oscillations are very close in time and hence it is almost impossible to disentangle the underneath constant level from the gaussian wing contributions. In these cases the only way to proceed is to fit the light curve with an appropriate $G_N(t)$ function and then eliminate every gaussian curve in turn, comparing the $[N - 1]$ -gaussian components fit with the complete one to find the significance of the suppressed hump. An HR light curve example in which the “unperturbed” constant value of HR is not immediately identifiable at first glance is the light curve shown in Fig. 1 c, together with the corresponding best fit we obtained, representing the 10/12/2005 *Suzaku* observation of NGC 3516. In this case, within the observation duration no clearcut constant HR time interval is present and a definition of the constant level underneath the variation components is possible only through the fitting process: our best fit defines 3 gaussian components that can be easily recognized in the figure. For this specific case our result is confirmed by the spectral analysis (Ursini et al. 2014) from which the authors conclude that the three components shown in Fig. 1 c are originated by the interposition of an obscuring cloud and cannot be due to a change in the emitting source spectral index. This fact confirms the reliability of our procedure also in the cases in which the various components are rather mixed.

We point out that in cases like the present one, we have also attempted a fit allowing for negative values of A_n . Not always such attempts produce good fits, but in some cases, like for the observation of NGC 3516 discussed above, the fit in which the HR light curve is described by a constant level ($K_N = 0.65$) with additional positive gaussian curves ($A_n > 0$) and the one described by a constant level ($K_N = 1.38$) with additional negative gaussian curves ($A_n < 0$) are comparable, i.e. they result in almost equal values of the reduced χ^2 . However, the case with negative gaussian curves demands a high value for the HR constant level ($K_N = 1.38$) which could be reproduced, in a type 1.2 source like NGC 3516, only by a very low intrinsic photon index. Such a flat spectrum in an unabsorbed source is not consistent with the observed properties of this type of sources. This conclusion also holds for the other few sources for which a fit with negative gaussian curves was possible.

As described above, fits with “high” initial reduced χ^2 ($\chi^2_{r0} > 1.1$) are followed by a further fit and the significance of adding a new gaussian to the fit is computed. However, for some cases this procedure does not give improving results, since the F-test shows that the simpler model, i.e. the fit with a constant function, is a better representation of the data. We believe that for these HR light curves the high χ^2_{r0} value is most probably a consequence of a “degraded” quality of the data, rather than being due to the actual presence of variations.

Looking at Table 2, it is apparent that there are many sources for which the HR fit with a constant function is a good one, thus indicating that the light curve is basically constant in time. On the other hand there are several sources for which one or more observations show a better fit of the

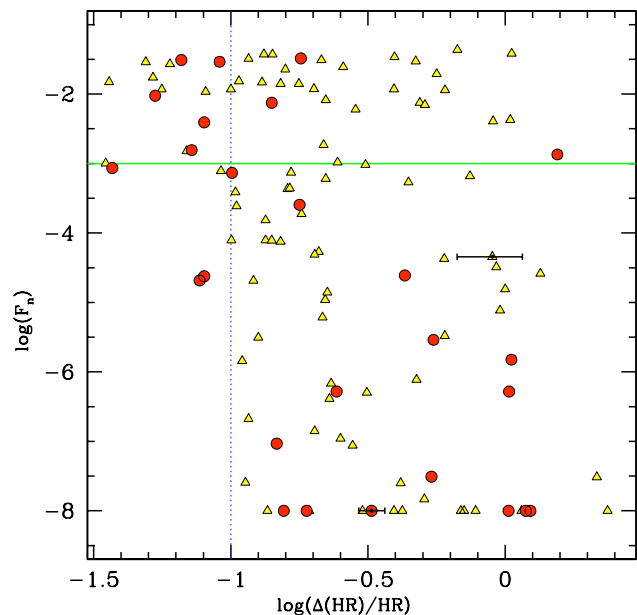


Figure 2. Significance value, F_n , for each hardness ratio variation fitted with a gaussian (see text for details), as a function of the corresponding relative peak height, $\Delta(HR)/HR$. Each variation is plotted as a triangle. Big circles represent the most significant event for each source in our sample. Note that for peaks with significance $F_n < 10^{-8}$ the value $F_n = 10^{-8}$ is shown in the figure. The 16 sources for which no significant ($F_n > 0.05$) event has been detected are not shown in the diagram. Representative error bars for $\Delta(HR)/HR$ are reported for a couple of events shown.

light curve when a time dependent trial function, i.e. $G_N(t)$, is used. These cases are good candidates for occultations.

Besides the statistical significance of HR variations, a second relevant indicator obtained by our fits is the ratio between the peak height of the n -th gaussian curve, and the underneath constant value (A_n/K_N in our model representation) which is a measure of the relative variation of the hardness ratio, $\Delta(HR)/HR$. The importance of this parameter will be clear from the analysis in the next Section, where we discuss the possible alternatives to occultations to reproduce the observed HR variations. Qualitatively, events with relatively low values of $\Delta(HR)/HR$, but with high statistical significance, may be found in light curves with particularly high S/N. In these cases, the spectral changes would be small despite the high statistical significance of the event. Therefore, the parameter $\Delta(HR)/HR$ is needed to better characterize the HR variation events.

The results of our analysis are shown in Fig. 2, where for each event the probability, F_n , that it is due to a statistical fluctuation is plotted against its $\Delta(HR)/HR$ ratio. Two representative error bars for the quantity $\Delta(HR)/HR$, shown in the figure, illustrate the error trend resulting from our analysis, i.e. the fact that smaller errors are associated to lower F_n values. It is also apparent that significant statistical ($F_n \leq 0.001$) HR variations are typically associated with $\Delta(HR)/HR > 0.1$, while this limit does not hold for HR humps associated to F_n values > 0.001 . The implications of this result will be analysed in Section 5.

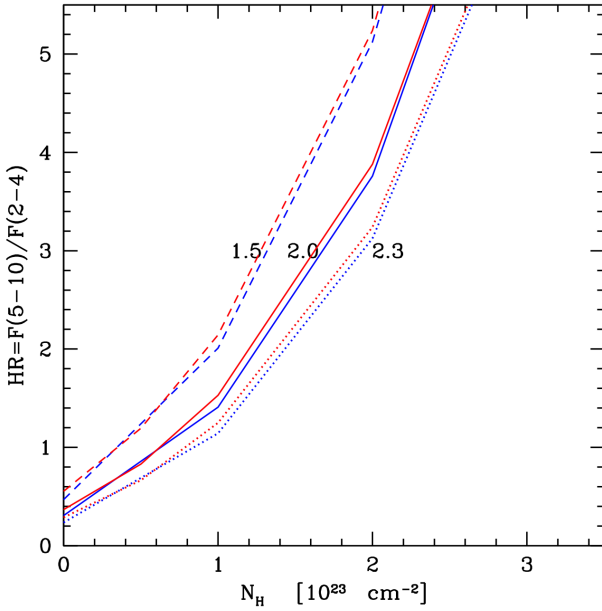


Figure 3. Synthetic hardness ratios as functions of the column density N_H for different values of the spectral index γ and for $C_F = 1$ and $R = 0$. For each γ , convolutions with the *XMM* (blue lines) and *Suzaku* (red lines) response matrices are shown.

4 INTERPRETATION OF THE ANALYSIS

The possible interpretations of humps in HR light curves as due to occultation by interposing clouds must be confirmed through a complete spectral analysis. For some sources in our sample this analysis has already been done. For example, as reported above, Risaliti et al. (2011) interpret as eclipses three strong variations in the hardness ratio light curve of Mrk 766 during *XMM* observations of 23 and 25 May 2005. The same interpretation has been confirmed by detailed analyses of HR variations observed in other sources (e.g. NGC 4151, Puccetti et al. 2007; NGC 4395, Nardini & Risaliti 2011; NGC 1365, Risaliti et al. 2007, 2009).

Here we discuss the main possible sources of HR variability, and we test our interpretation on two light curves for which we already performed a complete spectral analysis. All the results shown in this Section are obtained through the convolution of the theoretical models with the *XMM*-EPIC/PN response matrix, i.e. accounting for the effects of the energy-dependence of the effective area. Since the result depends on the specific instrument, when needed, the convolution is performed separately for the *XMM-Newton*-EPIC/PN, and the *Suzaku*/XIS instruments. In the following, we shortly call the quantities resulting from this procedure as “synthetic”.

A complete analysis of the hardness ratio variability implies the analysis of its dependence on γ , N_H , the cloud covering factor, C_F , and the ratio between the normalization of the reflected to the direct power law components, R , that is the evaluation of $HR \equiv HR(\gamma, N_H, C_F, R)$. As a first insight, the general behaviour of HR for different column densities and photon indexes is shown in Fig. 3. The visual analysis of Fig. 3 reveals several significant properties of our indicator:

- The value for unobscured sources is of the order of 0.4,

with little dependence on the photon index.

- The dependence on the photon index is weaker than that on the column density: the plotted lines refer to the whole observed range of photon indexes in nearby AGNs, nevertheless their distance in the $HR - N_H$ plane is not large, compared with the range of HR corresponding to variations of column density of the order of 10^{23} cm^{-2} .

To better quantify the different origins of HR variability and in order to compare our “synthetic” results with those of the data analysis shown in Fig 2, we computed for the hardness ratio function, $HR \equiv HR(\gamma, N_H, C_F, R)$, its fractional variability, $\Delta(HR)/HR$, with respect to each of the independent variables in turn, keeping all other variables constant. In the next Subsections we investigate these issues in more detail.

4.1 Effects of spectral index changes

The obvious objection to the interpretation of humps present in the HR light curves in terms of interposing clouds is that a spectral change, namely a decrease in the spectral index value, γ , of the X-ray emitting source, would produce the same effect. In this framework, the humps in the HR light curves could be the result of an episodic hardening of the emitted spectrum.

In the hypothesis that HR changes are only due to spectral index changes, we tested several cases maintaining $C_F = 1$ and $R = 0$. We noticed that for any given variation of photon index γ , we observe the highest fractional change $\Delta(HR)/HR$ in unobscured sources. Therefore, we concentrated on spectra with $N_H=0$, in order to explore the highest possible variations and hence we evaluated

$$\left[\frac{\Delta(HR)}{HR} \right]_{\gamma} = \frac{HR(\gamma - \Delta\gamma, 0, 1, 0) - HR(\gamma, 0, 1, 0)}{HR(\gamma, 0, 1, 0)} \quad (2)$$

where $HR(\gamma, 0, 1, 0) \equiv HR(\gamma, N_H = 0, C_F = 1, R = 0)$.

In Fig. 4 we present synthetic $\Delta(HR)/HR$ values obtained starting from different values of γ , and corresponding to three variations. Since we assume a positive $\Delta\gamma$, a decrease of the spectral index value results in an increase in HR , as Fig. 4 shows. In addition, these computations show two interesting facts: 1) the effect of γ variability is nearly the same for *XMM-Newton* and *Suzaku* spectra. This is evident also in Fig. 3 and it is due to the similarity of the dependence of the effective areas on energy for the two instruments. As a consequence, from now on we show only the results for *XMM-Newton*. Anyway, in all the cases discussed here we computed the synthetic quantities for both the observatories; 2) the effect of a variation of γ is almost independent of the starting value of γ . This effect is also due to the smooth behaviour of the effective area as a function of energy. Moreover, the measured $[\Delta(HR)/HR]_{\gamma}$ scales almost linearly with $\Delta\gamma$. As a consequence, we can approximate $[\Delta(HR)/HR]_{\gamma} \sim \Delta\gamma$ for every value of γ .

The figure also shows two square points obtained from *XMM* synthetic models for $\Delta(HR)/HR$ in the case of a constant non zero N_H , i.e. $N_H = 2 \times 10^{23} \text{ cm}^{-2}$, taken as representative value for Type 2 sources. These two points refer to the case of $\Delta\gamma = 0.2$ and therefore confirm what previously noticed, i.e. that the curves computed for $N_H = 0 \text{ cm}^{-2}$ and relative to Type 1 sources, those drawn in

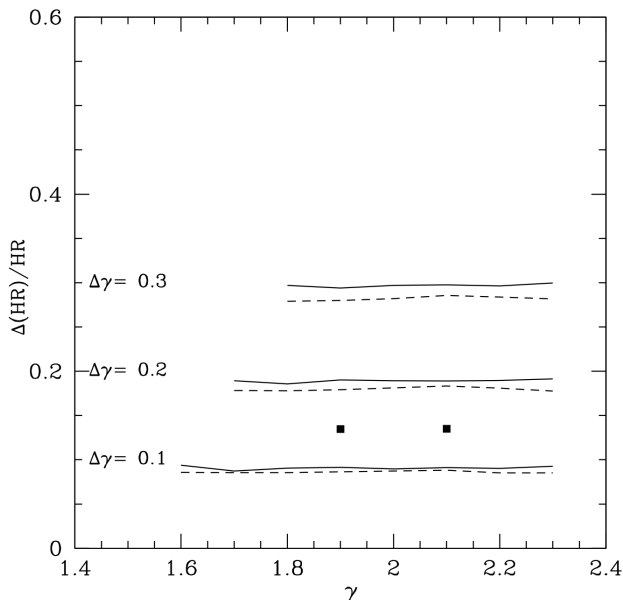


Figure 4. Upper limits of $[\Delta(HR)/HR]_\gamma$ values obtained from synthetic *XMM* (continuous lines) and *Suzaku* (dashed lines) spectra. Curves are labelled with the corresponding $\Delta\gamma$. The two square points refer to the case $\Delta\gamma=0.2$ for *XMM* synthetic model and show the effects of a constant non zero N_H , i.e. $N_H = 2 \times 10^{23} \text{ cm}^{-2}$.

Fig. 4, represent an upper limit to changes in HR curves due to spectral index variations.

We have reported in Fig. 4 the cases in which $\Delta\gamma \leq 0.3$. However, we do not expect any $\Delta\gamma \geq 0.1$ during individual observations, based on the two following arguments.

- Sobolewska & Papadakis (2009), and Papadakis et al. (2009), report a γ -intrinsic flux correlation in a sample of bright AGN (most of their sources are included in our sample), based on hundreds of snapshot Rossi-XTE observations over a period of more than 10 years. This correlation is obtained from a power law fit of each spectrum, so the physical origin of the correlation is not a-priori clear (for example, variable absorption could play a role, with a flatter spectrum and a lower flux associated to more absorbed states). However, even assuming an intrinsic γ -flux correlation, in most cases the slope of the dependence is flat enough to imply a photon index variation $\Delta\gamma < 0.1$ in the flux variability range observed in single observations (an exception is NGC 4051, which is known to show large flux and photon index variability, associated to either variable absorption or changes in the reflection fraction (Ponti et al. 2006)).

- In order to check this important point, we performed a complete spectral analysis on a subsample of five bright unobscured AGNs with significant HR variability (those with no spectral variability obviously do not need any check to confirm the constancy of γ). In this study, presented in the second paper of this series (Ursini et al. 2014) we fully confirm that all the cases with $\Delta(HR)/HR > 0.1$ are best reproduced through occultation events, while the variability in the only source in the sample with $\Delta(HR)/HR < 0.1$ can be also explained through intrinsic variability of γ .

4.2 Effects of large flux variations

A possible source of hardness ratio variability may be extreme *flux* variability. In most nearby AGN, a cold reflection component is observed, with a 2-10 keV flux of a few percent of that of the intrinsic emission. The total observed spectrum is therefore obtained adding these two components. If the total spectrum is fitted with a single power law, the measured best fit photon index is close, within a few percent, to that of the intrinsic power law, the contribution of the reflection being small. However, if the reflector is far enough from the central source, a strong decrease of the intrinsic flux may propagate to the reflection components in longer times than the intrinsic variability time scales. In this scenario, it would be possible to observe quite large reflection/intrinsic emission ratios. Since the reflection component is much harder than the intrinsic power law in the 2-10 keV range (e.g. Magdziarz & Zdziarski 1995, Murphy & Yaqoob 2009) we would then observe a significant change of the observed HR . This is indeed one of the explanations suggested by Sobolewska & Papadakis (2009) to explain the γ -flux correlation over large flux variations. In order to explore this possibility we computed the synthetic quantity $\Delta(HR)/HR$ assuming a configuration in which we have an intrinsic power law continuum with constant (fixed) photon index, $\gamma=2$, and no intrinsic absorption, together with a Compton-thick reflector covering 2/3 of the solid angle as seen from the central source, originating the reflected emission component. Technically, we simulated this scenario through a PEXRAV model (Magdziarz & Zdziarski 1995) with a ratio R between the normalizations of the reflected and intrinsic components $R=1.35$. Since the actual reflectors are on average less efficient than the one assumed here, the results of our procedure can be considered upper limits of the observable HR variations. Within this framework, we suppose that, due to intrinsic source variability, the intrinsic flux decreases from a “high” value F_{MAX} to a value F_{OBS} and we assume that within the intrinsic variability time-scale (i.e., the lapse of time in which the intrinsic flux value drops) the reflection component stays constant, because the propagation time for the intrinsic flux variation to reach the reflector distance is longer than the intrinsic variability time-scale. If this is the case, the synthetic HR variations are induced by the different *relative* contribution of the reflected component in the two conditions for the intrinsic flux. The results are shown in Fig. 5.

It is clear that the level of X-ray flux variability usually observed in AGNs, on time scales of hours-days, is not enough to produce high changes of HR .

4.3 Effects of N_H variations

The same procedure described in Section 4.1 can be applied to the case of interposing clouds with different covering factor, C_F , but still with $R = 0$.

As in the previous case the quantity which is more significant for the comparison with the observed light curves is the relative HR variation with respect to the unperturbed case, i.e. the case with $N_H = 0$ for Type 1 sources or the case in which matter with intrinsic column density $\tilde{N} = 2 \times 10^{23} \text{ cm}^{-2}$ (chosen as representative for the case of Type 2 sources) covers the whole source. We have chosen a

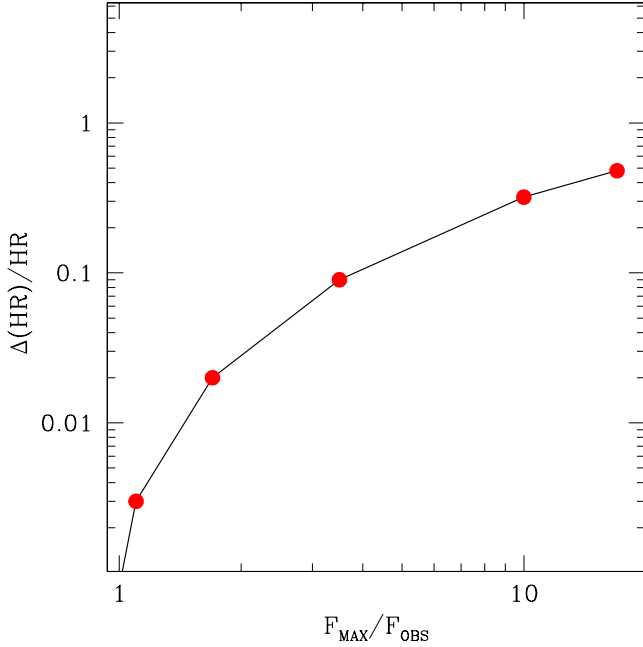


Figure 5. Computed $\Delta(HR)/HR$ corresponding to 2-10 keV intrinsic flux variations. To compute the synthetic quantity, we assume that the intrinsic flux drops from F_{MAX} to F_{OBS} , while the reflection component remains at a constant value, corresponding to the reflection of F_{MAX} by a Compton-thick reflector, covering $2/3$ of the solid angle.

representative “mean” value, $\gamma = 2$, for the spectral index. In these two cases, HR variations read

$$\left[\frac{\Delta(HR)}{HR}\right]_{N_H} = \frac{HR(2, N_H, C_F, 0) - HR(2, 0, 1, 0)}{HR(2, 0, 1, 0)} \quad (3)$$

and

$$\left[\frac{\Delta(HR)}{HR}\right]_{N_H + \tilde{N}} = \frac{HR(2, N_H + \tilde{N}, C_F, 0) - HR(2, \tilde{N}, 1, 0)}{HR(2, \tilde{N}, 1, 0)} \quad (4)$$

for Type 1 and Type 2 sources, respectively. Note that here and in the following the covering factor C_F always refers to eclipsing cloud column density and not to the intrinsic column density in Type 2 sources.

In order to properly “simulate” actual occultations, we must consider the possibility that only part of the X-ray source could be eclipsed by the obscuring cloud. This is expected if the eclipsing cloud is smaller than, or the same size as, the X-ray source, as it has been already observed in the individual sources cited in the Introduction. Therefore, we repeated our procedure for deriving synthetic quantities for several different values of the covering factor (C_F) to the central X-ray source.

Figure 6 shows the synthetic quantity $\Delta(HR)/HR$ for Type 1 and Type 2 sources as a function of the eclipsing cloud column density, N_H , for fixed $\gamma = 2$, for the case of *XMM* instrument. Continuous lines refer to Type 1 sources and show how the synthetic quantity $\Delta(HR)/HR$ changes in different cases corresponding to different covering factors of the X-ray emitting source, ranging from the case of a complete eclipse ($C_F = 1$) down to a case in which half of the source is obscured ($C_F = 0.5$). For the case of Type 2 sources (shown as dashed lines) we take into account an intrinsic constant absorption with $\tilde{N} = 2 \times 10^{23} \text{ cm}^{-2}$ plus

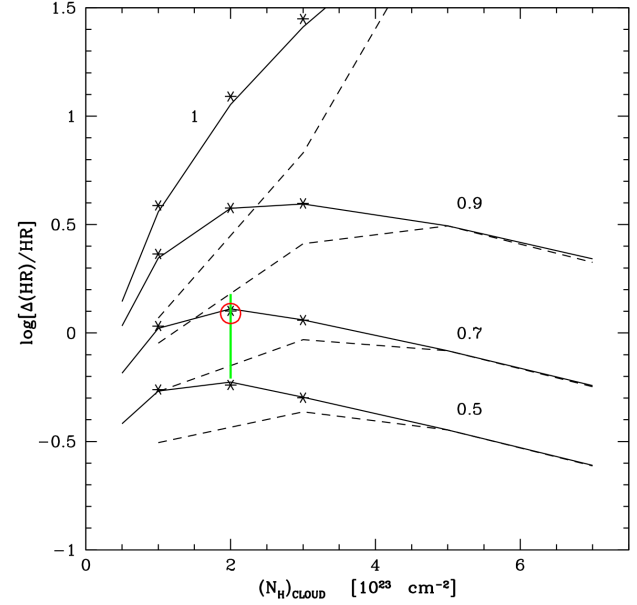


Figure 6. $\Delta(HR)/HR$ values obtained from synthetic *XMM* spectra as a function of occulting cloud column density, N_H , for different values of the covering factor and fixed $\gamma = 2$. Continuous lines refer to the case of unabsorbed Type 1 sources (see Eq.(3)); dashed lines refer to the case of Type 2 sources with uniform intrinsic absorption $\tilde{N} = 2 \times 10^{23} \text{ cm}^{-2}$ (see Eq.(4)). Curves are labelled with the covering factor value. Asterisks show the same results for Type 1 sources with a different spectral index, namely $\gamma = 2.3$. The green segment indicates the range of values deduced from the spectral analysis for a specific observation of NGC 1365 (see text for details) and the red circle the value of $\Delta(HR)/HR$ derived in this paper from the corresponding HR light curve.

the partial ($C_F < 1$) to total ($C_F = 1$) cloud obscuration (see Eq.(4)).

Some tests, shown as asterisks in the figure, have been also done for the case of Type 1 sources with a different spectral index value, namely $\gamma = 2.3$. It is evident that the change in the spectral index does not modify the results. The same analysis has been performed also for *Suzaku* and the results confirm those shown for *XMM*.

These results clearly show that HR light curves with significant and high humps ($\Delta(HR)/HR \gtrsim 0.3$) can be easily explained by clouds crossing the line of sight and eclipsing at least half of the X-ray source ($C_F \gtrsim 0.5$).

4.4 Comparison with detailed spectral analysis

The final result of the previous analysis, as it is apparent from the comparison of Figures 4, 5 and 6, is that large variations in the HR light curves cannot be due to either spectral index variations or large flux variations, while interposing clouds with different covering factor can imply large $\Delta(HR)/HR$.

In order to better illustrate our analysis, and to test our conclusion in real cases, we analyze in more detail two observations for which we already performed a complete time-resolved spectral analysis. We choose the long 2005 *XMM-Newton* observation of Mrk 766 (Risaliti et al. 2011) where we found three clear occultations, due to three different

eclipsing clouds, and the *Suzaku* observation of NGC 1365 reported in Maiolino et al. 2010. To compare the spectral analysis results with those obtained with our method, we must take into account that in our analysis the hardness ratio variations are described by a gaussian curve and, hence, each value we derive to quantify HR humps is related to this specific type of description. In practice, we can compare the $\Delta(HR)/HR$ values derived here with those deduced from the spectral analysis only on time scales corresponding to intervals as long as the gaussian half maximum width and centered on the maximum of the observed HR hump.

Mrk 766: The observations during which the occultations occurred are the first and second in 2005 (Risaliti et al. 2011 Table 2). Our best fits include two highly significant events in the first observation, and one in the second observation. In these cases the statistics is good enough to allow a detailed analysis (Risaliti et al. 2011) of the C_F and N_H changes during each occultation, with a time resolution of ~ 10 ks, therefore for each event we obtained a range of values for C_F and N_H . We also ruled out a significant contribution from continuum variability: a fit allowing only for spectral index variability is ruled out at high statistical significance in each of the three events. Moreover, each event has been fitted with a model where all the components discussed in the previous Subsections (photon index, absorption, relative reflection/intrinsic flux ratio) were free to vary, and the best fit solution is compatible with constant photon index and variable absorption. In order to compare Risaliti et al. 2011 results with those of our method, as explained above, we must select in their Table 3 the time intervals corresponding to our gaussian curves, i.e. $\Delta t(1) = [0 - 3 \times 10^4]$ s and $\Delta t(2) = [7 \times 10^4 - 1 \times 10^5]$ s for the first observation and $\Delta t(3) = [5 \times 10^3 - 2 \times 10^4]$ s for the second observation. The best fit values for covering factor and column density, obtained from spectral analysis for the three events, are $N_H(1)=0.9-2.5 \times 10^{23} \text{ cm}^{-2}$, $C_F(1) = 0.82 - 0.89$; $N_H(2)=1.7-1.84 \times 10^{23} \text{ cm}^{-2}$, $C_F(2) = 0.84 - 0.97$; $N_H(3)=0.6-1.9 \times 10^{23} \text{ cm}^{-2}$, $C_F(3) = 0.60 - 0.85$.

If we compare these results with the synthetic quantities in Fig. 6, for the N_H and C_F intervals quoted above, we expect: $[\Delta(HR)/HR](1)=1.5-4$; $[\Delta(HR)/HR](2)=2.2-10$; $[\Delta(HR)/HR](3)=0.5-2.5$. These values must be compared with those derived from the totally independent method of this paper, i.e. with the results of the gaussian fit of the hump in HR light curves. From Table 2 we find that the corresponding values are $[\Delta(HR)/HR](1)=2.15$; $[\Delta(HR)/HR](2)=2.36$; $[\Delta(HR)/HR](3)=1.03$ in agreement with the above intervals.

NGC 1365. The comparison described above for Mrk 766 has been repeated for the case of an obscured AGN, NGC 1365 ($N_H \sim 2 \times 10^{23} \text{ cm}^{-2}$). This specific case is also shown in Fig. 6 as an example of the method we followed. The light curve for this same observation is the one shown in Fig. 1b and shows a strong variability of HR with a large peak around 2×10^5 s. A complete spectral analysis (Maiolino et al. 2010) demonstrated that in the time interval $[1.5 \times 10^5 - 2.2 \times 10^5]$ s this variation is due to a cloud crossing the line of sight, with a column density of $\sim 2 \times 10^{23} \text{ cm}^{-2}$, and a covering factor $C_F = 0.65 - 0.9$. These values are shown in Fig. 6 as a green segment connecting the intersection of the dashed curves with constant covering factor ($C_F = 0.65$ and $C_F = 0.9$) for the fixed

value $N_H = 2 \times 10^{23} \text{ cm}^{-2}$. The corresponding range of $\Delta(HR)/HR$ is, from Fig. 6, $\Delta(HR)/HR=0.6-1.5$, in agreement with our result of Table 2 ($\Delta(HR)/HR=1.23$) shown as a red circle in the figure.

The comparisons described above clearly show that the analysis presented here provides results in agreement with complete spectral analyses. It is also apparent that from our analysis it is not possible to proceed in the opposite direction, i.e. derive two parameters (N_H and C_F) with only one observable ($\Delta(HR)/HR$).

5 RESULTS

In the previous Section we showed that most of the variability of the X-ray hardness ratio, HR , observed in local bright AGNs can be due only to occultations of clouds crossing the line of sight.

Based on this conclusion, we can analyze the results in Fig. 2, and qualitatively divide the variability events in four groups:

- 1) Low probability of chance fluctuation ($F_n \leq 10^{-3}$), and $\Delta(HR)/HR > 0.1$. These are events whose interpretation is unambiguous, and we expect to be able to confirm the occultations in all cases through time-resolved spectral analysis.
- 2) Low F_n , ($F_n \leq 10^{-3}$), and $\Delta(HR)/HR < 0.1$. These are cases in which the variability is not due to fluctuations, but the interpretation is less certain. A strong change of photon index, or an extreme flux variation, may produce the same effect as an occultation.
- 3) $F_n > 10^{-3}$, and $\Delta(HR)/HR > 0.1$. These are candidate occultations, for which the statistical significance of the HR variation is not high enough to rule out a statistical fluctuation.
- 4) $F_n > 10^{-3}$, and $\Delta(HR)/HR < 0.1$. These are marginal events, which cannot be confirmed through a spectral analysis due to low statistics, and where the spectral variation is modest. We expect that a fraction of these events are occultations (probably with a low covering factor), but we will conservatively assume that no absorption variation has been detected in these cases.

We note that the limiting values of $\Delta(HR)/HR$ and F_n are arbitrary, and rather conservative. Indeed, events with F_n of a few 10^{-3} are still quite significant (the customary $3\text{-}\sigma$ limit corresponds to $F_n = 3 \times 10^{-3}$), and our analysis of the photon index variability suggests that most of the events with $\Delta(HR)/HR > 0.1$ are due to occultations. However, we adopt this conservative approach based on practical considerations: 1) the value $F_n = 10^{-3}$ roughly corresponds to the limit where, based on our past experience, we are sure to be able to confirm the results through time-resolved spectroscopy; 2) the value $\Delta(HR)/HR > 0.1$ is a safe upper limit; at any rate we plan to perform time-resolved spectroscopic analysis of the cases with low F_n and $\Delta(HR)/HR < 0.1$, in order to complement the present analysis based only on light curves and to test if the thresholds adopted here for F_n and $\Delta(HR)/HR$ are confirmed.

In summary we have 15 out of 42 sources with highly probable occultation events ($\Delta(HR)/HR > 0.1$ and $F_n \leq 10^{-3}$), 3 sources with $\Delta(HR)/HR < 0.1$ and $F_n \leq 10^{-3}$, i.e. cases with highly significant variability events, which may be due either to occultations or to intrinsic variability, and

24 sources with no strong evidence for spectral variability. From these numbers we conclude that at least 1/3 of local AGNs shows occultations on time scales of the order of, or shorter than, the observing time.

We can further refine this analysis by comparing our results with the physical occultation time scales of each source, under the hypothesis that the observed spectral variations are due to broad line clouds crossing the line of sight.

We want to give an estimate of the eclipse duration timescale for each of the sources listed in Table 1. The simplest and most effective (in terms of source coverage due to the intervening cloud) geometry for the eclipse event is the one in which, assuming for simplicity both source and cloud as spherical, the cloud centre moves on a trajectory that intercepts the source centre; in this case, following Risaliti et al. (2007), the eclipse timescale can be evaluated as $2(R_X + R_{cloud})/v_{cloud} = 2R_X/v_{cloud}(1 + R_{cloud}/R_X)$, where R_X is the X-ray source radius, R_{cloud} is the radius of the cloud, and v_{cloud} is the cloud velocity. However, in general we must expect a broad range of different geometrical configurations due both to varied cloud paths and to different size of the clouds themselves. In fact, in our framework, still maintaining the simplifying hypothesis of spherical geometry for source and clouds, we expect clouds to cross the line of sight to the source, and obscure it, moving on different trajectories (that we suppose locally rectilinear for simplicity), thus allowing for a distance, d , between the trajectory of the moving cloud centre projected on the plane of the sky and the source centre, $d = f_d R_X$, where f_d is a non-dimensional parameter, whose values must be $0 \leq f_d < (1 + R_{cloud}/R_X)$ in order to have an eclipse event at all. This of course affects both the resulting duration of the eclipse and the corresponding maximum covering factor, $(C_F)_{max}$, attained during the passage. As for the size of the eclipsing cloud, that we parameterize with its radius R_{cloud} , any assumption on that just aims at defining an order of magnitude evaluation; at the present stage, only upper and lower *operative* limits exist for the cloud extension. In fact, eclipsing clouds are detectable with our method only if their physical and geometrical properties are such to produce an observable emission decrease and hence a hump in the *HR* light curve. Too large clouds would not be detectable, since their passage would produce too long eclipsing times which could result longer than the available light curve duration (see below). On the other hand, too small clouds would leave the source emission almost unaffected. Ultimately, based on our analysis of model convolution with response matrices of the instruments, we find that clouds with detectable effects on the source emission must produce maximum covering factors larger than 0.1 and this implies it must be $R_{cloud} \geq 0.3R_X$. Taking into account the considerations above, the timescale for the eclipse duration, Δt_{ecl} , that we want to evaluate as the time a BLR cloud takes to cross the X-ray source (Risaliti et al., 2007), can be expressed as

$$\Delta t_{ecl} \simeq 2 Q \frac{R_X}{v_{cloud}},$$

where $Q \equiv Q\left(\frac{d}{R_X}, \frac{R_{cloud}}{R_X}\right)$ is a factor that depends on the values of d/R_X and R_{cloud}/R_X . In order to define the most representative estimate of the factor Q , we have explored the portion of parameters space identified by the ranges

$0.3 \leq R_{cloud}/R_X \leq 1$ and $0 \leq d/R_X \leq (1 + R_{cloud}/R_X)$, with the constraint that the eclipsing event produces a maximum covering factor ≥ 0.1 , *i.e.*, an observable variation effect in the hardness ratio light curve. From this analysis, we conclude that $Q \simeq 1.5$ can be chosen as an average, representative value for the resulting range, and, as a consequence, we adopt this value for our estimate of the duration of the source obscuration in the cloud passage, that is the eclipse timescale

$$\Delta t_{ecl} \simeq 3 \frac{R_X}{v_{cloud}} \simeq 7.5 R_S / v_{cloud},$$

where $R_S = 2GM_{BH}/c^2$ is the Schwarzschild radius and we have assumed the source diameter $D_X = 2R_X \simeq 5R_S$. This last assumption is supported also by the recent results of a detailed study of one of the sources in our sample, namely IGR J21277+5656 (also called SWIFT J2127.4+5654), by Sanfrutos et al. (2013); in this work, time resolved spectral analysis of the source, interpreted as a partial eclipse by an intervening BLR cloud-like absorber, enables the authors to constrain the size of the X-ray emitting region, that turns out to be $D_X \leq 10.5 GM_{BH}/c^2 = 5.25R_S$, when adopting $M_{BH} \sim 1.5 \times 10^7 M_\odot$, a value estimated from single-epoch optical spectroscopy.

For cloud velocities two different estimates have been compared.

i) In Type 1 sources, cloud velocity can be directly estimated from the broad line widths. Among the average speed and dispersion values found in quasars of the Sloan Digital Sky Survey (Ahn et al. 2012) we note that more than 90% of the SDSS quasars have line widths within a 2000-6000 km/s range, *i.e.* with a smaller dispersion with respect to the central value than the uncertainty on the black hole mass and/or on the size of the X-ray source. Therefore, we have assumed $v_{cloud} = 4000$ km/s, as representative cloud speed for all sources, except for the three NLS1 sources for which $v_{cloud} = 1000$ km/s has been assumed.

ii) The cloud velocity can be estimated also in the hypothesis that X-ray obscuring clouds undergo a keplerian motion around the central black hole, *i.e.* $v = (GM_{BH}/R_{BLR})^{0.5}$, and that the Bentz et al. (2013) radius-luminosity correlation, $R_{BLR} \simeq 33.6 [L_{5100}/10^{44}]^{0.533}$ light days, holds for every type of source in our sample. The use of the above expression needs an estimate of the 5100Å luminosity, L_{5100} , which, for several sources in our sample, is not available from observations and must be in some way evaluated. Our choice was to adopt the values of L_{5100} present in literature, when possible (Bentz et al. 2013, Winter et al. 2010), and, otherwise, derive L_{5100} by means of the optical to X-ray spectral index derived by Young et al. (2010), where the monochromatic 2 keV flux has been obtained by extrapolating the measured 15-195 keV flux from the Swift/BAT 54 month catalogue (Cusumano et al. 2010) using the spectral index given in the same catalogue. From the value of L_{5100} and using the relationships quoted above, an approximate value for the cloud speed and hence for the eclipsing time can be derived for each of the sources in Table 1, except for 2MASX J04532576+0403416, for which no value for the central black hole mass is available in the literature.

We find that the eclipsing time values evaluated by using L_{5100} , taken from literature or estimated as described

above, and the values obtained assuming a constant cloud velocity are of the same order of magnitude, since the ratio of the two estimates is in the range [0.3-4] for all the sources in our sample (apart from a couple of exceptions, MCG 06-30-15 and ESO 141+55, for which the ratio is ~ 5) and for about 80% of the sources it is in the narrower range [0.4-2]. In the following we always adopt for the estimate of the crossing time Δt_{ecl} the luminosity-based method and the derived values are listed in Table 1 for each source of our sample.

The estimated Δt_{ecl} can be correlated with the results of our light curve analysis. In Figure 7 we plot the probability F_n for each event, versus the ratio, $\Delta t_{ecl}/\Delta t_{eff}$, between Δt_{ecl} and the effective duration of the observation, Δt_{eff} . We must stress here that, once we have performed our fit on a given *HR* light curve, we do have an evaluation of the timescale for each variation we fitted with a gaussian shape, defined by the parameter measuring the gaussian width. In doing the fit, the effective duration of each single observation poses a limit on the width of the fitting functions we use to match the observed hardness ratio variations in the corresponding light curve: we can reliably fit only variations that are clearly visible within the duration of the light curve, *i.e.*, those occurring on a timescale that is $\leq 2\Delta t_{eff}$. For larger values, we could in principle still be able to measure significant spectral variations, however our method requires at least \sim half of an eclipse to be monitored in order to have a significant gaussian component in our fits of the light curves. In the framework of our physical interpretation, our estimate of the eclipse timescale Δt_{ecl} for a given source should be representative of expected timescales for *HR* variations, although we may envision significant deviations of the actual observed variation timescales, due to the simplifying assumptions in our calculation above. Keeping in mind these considerations, the plot in Fig. 7 shows the two most relevant results of our work.

1) We assume that the operative limit on observable and analysable hardness ratio variations timescale ($\leq 2\Delta t_{eff}$) can be extended also to our estimate of a typical eclipsing time for a source, Δt_{ecl} , and we trace a vertical line for $\Delta t_{ecl}/\Delta t_{eff} = 2$ in Fig. 7. This figure shows that no highly significant ($F_n \leq 10^{-3}$) events are detected with $\Delta t_{ecl}/\Delta t_{eff} > 2$. We point out that, despite the large uncertainties in our estimates, the quantities involved in this comparison, *i.e.* the statistical significance of the variations, the estimated BLR eclipsing times, and the actual observing times, are both observationally and physically unrelated. Therefore, a clear result such as the lack of events in the bottom-right part of the plot in Fig. 7 represents a strong self-consistency check both of our eclipse-based interpretation of the spectral variations, and of our hypothesis that such eclipses are due to BLR clouds.

In order to clarify the relevance of the result shown in Fig. 7, it is useful to mention that we analysed the distribution of values of the ratio $\Delta t_{ecl}/\Delta t_{eff}$ estimated for all the observations in our sample and we found this distribution to be almost symmetric with respect to $\Delta t_{ecl}/\Delta t_{eff} \simeq 1$; more specifically, we found that the number of observations corresponding to $\Delta t_{ecl}/\Delta t_{eff} \geq 2$ is about 39% of the total number of observations; as a consequence, the absence of significant *HR* variation events in the lower right portion of

the plot in Fig. 7 cannot be explained with a scarcity of observations with $\Delta t_{ecl}/\Delta t_{eff} \geq 2$. In fact, the only events we have been able to fit for observations with $\Delta t_{ecl}/\Delta t_{eff} > 2$ and appearing in the plot are located in the upper right portion, since, according to our method of analysis, their significance is low. It is important to point out that the absence of statistically significant *HR* variation events in observations with $\Delta t_{ecl}/\Delta t_{eff} \geq 2$ is not a truism, since our procedure would in principle allow for the detection of significant events in a *HR* light curve, even though for that same observation $\Delta t_{ecl} \geq 2\Delta t_{eff}$. In fact, the only limit to detect an event would be on the actual duration of the event itself, that is on the width measure of the appropriately fitting gaussian component: we can in principle always fit *HR* variation events whose duration measure ($\simeq w_n$, see Section 3.3) is $\leq 2\Delta t_{eff}$, but, for an observed light curve with $\Delta t_{ecl} \geq 2\Delta t_{eff}$, in those cases it would be $w_n < \Delta t_{ecl}$ or even $\ll \Delta t_{ecl}$. No such statistically significant events turn out to exist from our analysis and this is right what one would expect if (and only if) the origin of significant *HR* variations were indeed due to a cloud-like structure eclipsing the source while crossing our line of sight to the source itself.

2) From an analysis of the left part of the plot (*i.e.* the only region of the parameter space where it is possible to see occultations due to BLR clouds), $\Delta t_{ecl}/\Delta t_{eff} < 2$, we find 16 sources with at least one highly significant event ($F_n \leq 10^{-3}$). Out of this subgroup, only two objects have $\Delta(HR)/HR < 0.1$, thus not excluding the possibility of intrinsic spectral variability. The upper part of the diagram ($F_n > 10^{-3}$) contains the most significant event for only one source; in addition other 6 sources exist in our sample having $\Delta t_{ecl}/\Delta t_{eff} < 2$ (not shown in the figure since they do not have any significant hump characterized by $F_n < 0.05$ in their *HR* light curves). Therefore the fraction of sources for which is $\Delta t_{ecl}/\Delta t_{eff} < 2$ and having detected X-ray occultations is $14/26=54\%$. This confirms that eclipses by BLR clouds are common among AGNs. This estimate should be regarded as a lower limit, for several reasons.

a) Our analysis method is relatively fast and homogeneous for the whole sample. However, a more *ad-hoc* analysis of individual light curves could reveal more significant variability events. Moreover, the significance of the possible column density variation, as measured in a time-resolved spectral analysis, is of course related to the significance of the hardness ratio variation in the light curve, but with some dispersion. This is due to the degeneracy among model parameters in the spectral fits, which are dependent on the details of the model and on the data quality, and should be estimated on a case-by-case basis. Our experience suggests that the value $F_n=10^{-3}$ is a reasonable threshold: events with a higher statistical significance typically are confirmed by a complete spectral analysis, while in less significant ones the variations of model parameters such as column density and continuum spectral index are degenerate.

b) Significant variability events may be detected comparing the spectral analysis of *different* observations. A known example is the Type 2 Seyfert Galaxy NGC 7582, for which the hypothesis of obscuring clouds has been supported by the comparison of two XMM-Newton observations taken four years apart (Piconcelli et al. 2007) and by comparing

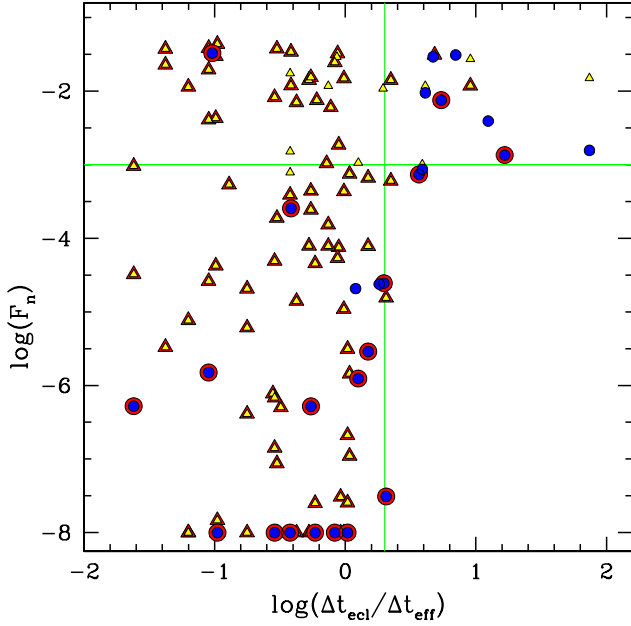


Figure 7. Statistical significance of the hardness ratio variations, F_n as a function of $\Delta t_{ecl}/\Delta t_{eff}$, where Δt_{eff} is the observation length, and Δt_{ecl} is the duration of the eclipse estimated assuming that the HR variation is due to a broad line cloud covering the source (see text for detail). Each event is represented by a triangle. Circles indicate the most significant event for each source in the sample. Big, red contours are for events with $\Delta(HR)/HR > 0.1$. Note that for peaks with significance $F_n < 10^{-8}$ the value $F_n = 10^{-8}$ is shown in the figure.

the spectral analysis of a series of short *Suzaku* observations (Bianchi et al. 2009). On the contrary, for this source the only observation meeting the criteria of our sample and analyzed with our method does not show any significant variability.

c) Occultations by BLR clouds may occur, but we could have missed them in our observation sample. This is for example the case of NGC 4388, a Type 2 Seyfert galaxy for which all the existing *XMM* observations do not enter in our sample since last less than 80 ks (our lower limit), and the analyzed *Suzaku* observation does not show any variability since it is well fitted by a constant ($\chi^2_0 = 0.99$). Hence, for this source we do not detect any significant variability whereas variability has been observed in the data obtained by a different instrument when the source was in a Type 1 unobscured state during a Rossi-XTE monitoring campaign (Elvis et al. 2004). It is interesting to notice that some of our most significant occultation events have been detected in the NLS1 Mrk 766 thanks to a particularly long *XMM-Newton* monitoring (6 orbits), but with a small fraction of the observing time affected by these events. Therefore, it is likely that a single ~ 100 ks long observation (as in most of our sources) would not detect any occultation in this source, even if it is one of our best cases.

6 CONCLUSIONS

The aim of this paper was to test on a larger sample the hypothesis of X-ray occulting clouds already proved for a small number of sources [see Risaliti (2010) and references therein] in recent years. Therefore, we have selected a statistically representative sample of bright X-ray AGNs for which long lasting *XMM* (> 80 ks) and *Suzaku* (> 50 ks) observations are available and, for each suitable observation, we have derived the hardness ratio (HR) light curve. In these HR curves we have identified any time interval where the HR is not constant but shows a hump and we have fitted these humps with gaussian curves in order to have a way to quantify the hump location, width and height over the constant HR level. We have also computed the statistical significance of the obtained fits, deriving for each gaussian curve its null probability, F_n from the F-test. The results of this analysis are shown in Table 2 and constitute the basis for the further analysis.

It is well known that the possible interpretations of humps in HR light curves as due to occultations by interposing clouds must be confirmed through a complete spectral analysis, as has been done in the above reported cases. However, the idea of this paper was to devise a method which could allow a first concise but faster analysis on a large number of sources. For this reason we have investigated the dependence of HR humps (in particular the height of each hump over the constant level represented by the fractional variation, $\Delta(HR)/HR$) on the cloud column density and covering factor and on the X-ray radiation spectral index. To quantify these dependences we have employed synthetic models deriving (see Figs. 4 to 6) a specific limit: humps with $\Delta(HR)/HR > 0.1$ cannot be due to spectral index variations but can be explained with the effects of crossing clouds. With this limit we can already say that a large number of the detected humps is originated by crossing clouds. This conclusion can be strengthened by the analysis of the theoretically deduced eclipsing times. In fact, for each source in the sample, we have computed the time necessary for a cloud with a diameter the order of $5 R_S$ and located at BLR distance to cross the central source and we have compared this time to each observation length.

The main results of our analysis, shown in Fig. 7, are the following. First, it is evident that there are not significant humps ($F_n \leq 0.001$) in the region corresponding to theoretical eclipsing times longer than twice the observation time. Since the choice of the physically relevant time-scale (Δt_{ecl}) appearing in the time ratio used for Fig. 7 follows from our eclipsing cloud interpretation of HR variability, the empty lower right region in Fig. 7 is a strong confirmation of this same physical interpretation. In fact, no other physical source of HR variability would imply a distribution of significant HR time variation events showing a dependence on the timescale for a BLR cloud to cross the X-ray source extension.

Secondly, Fig. 7 allows an evaluation of X-ray occultation frequency. Eclipses by BLR clouds seem very common in AGNs since in our sample the fraction of sources with good candidate X-ray occultations detected is 54%, among the sources for which $\Delta t_{ecl} \lesssim \Delta t_{eff}$.

In conclusion, our study of a statistically representative sample of AGNs prompts the validation of a method for the

identification of BLR cloud occultation events based on the analysis of the *HR* light curves, and the results we obtain give full support to the physical interpretation of *HR* time variability in terms of X-ray source occultations by BLR-like clouds crossing the line of sight to the source itself.

ACKNOWLEDGEMENTS

This work has been partly supported by grants NASA NNX08AN48G, PRIN-MIUR 2010-2011 "The dark Universe and the cosmic evolution of baryons: from current surveys to Euclid" and PRIN-INAF 2011 "Black hole growth and AGN feedback through the cosmic time".

REFERENCES

- Ahn C.P. et al., 2012, *ApJS*, 203, 21
 Antonucci R., 1993, *ARA&A*, 31, 473
 Beckmann V. et al., 2009, *A&A*, 505, 417
 Bentz M.C. et al., 2006, *ApJ*, 651, 775
 Bentz M.C. et al., 2013, *ApJ*, 767, 149
 Bianchi S., Piconcelli E., Chiaberge M., Bailn E.J., Matt G., Fiore F., 2009, *ApJ*, 695, 781
 Bianchi S., Maiolino R., Risaliti G., 2012, *Advances in Astronomy Volume 2012*
 Burlon D., Ajello M., Greiner J., Comastri A., Merloni A., Gehrels N., 2011 *ApJ*, 728, 58
 Cusumano G. et al., 2010, *A&A*, 524, 64
 Denney K.D. et al., 2006, *ApJ*, 653, 152
 Denney K.D. et al., 2010, *ApJ*, 721, 715
 Elvis M., Risaliti G., Nicastro F., Miller J.M., Fiore F., Puccetti S., 2004, *ApJ*, 615L, 25
 Grandi P., Malaguti G., Fiocchi M., 2006, *ApJ*, 642, 113
 Grier C.J. et al., 2012, *ApJ*, 755, 60
 Guainazzi, M., Bianchi S., Matt G., Dadina M., Kaastra J., Malzac J., Risaliti G., 2010, *MNRAS*, 406, 2013
 Haardt F., Maraschi L., 1993, *ApJ*, 413, 507
 Kuo C.Y. et al., 2011, *ApJ*, 727, 20
 Lamer G., Uttley P., McHardy I. M., 2003, *MNRAS*, 342L, 41L
 Magdziarz P., Zdziarski A.A., 1995, *MNRAS*, 273, 837
 Maiolino R., Rieke G. H., 1995, *ApJ*, 454, 95
 Maiolino R. et al., 2010, *A&A*, 517, 47
 Malizia A. et al., 2008, *MNRAS*, 389, 1360
 Middleton M., Done C., Schurch N., 2008, *MNRAS*, 383, 1501
 Miniutti G., Panessa F., de Rosa A., Fabian A.C., Malizia A., Molina M., Miller J.M., Vaughan S., 2009, *MNRAS*, 398, 255
 Nardini E., Risaliti G., 2011, *MNRAS*, 417, 2571
 Onken C.A. et al., 2007, *ApJ*, 670, 105
 Papadakis I.E., Sobolewska M., Arevalo P., Markowitz A., McHardy I.M., Miller L., Reeves J.N., Turner T.J., 2009, *A&A*, 494, 905
 Peterson B.M. et al., 2004, *ApJ*, 613, 682
 Peterson B.M. et al., 2005, *ApJ*, 632, 799
 Piccinotti G., Mushotzky R.F., Boldt E.A., Holt S.S., Marshall F.E., Serlemitsos P.J., Shafer R.A., 1982, *ApJ*, 253, 485
 Piconcelli E., Bianchi S., Guainazzi M., Fiore F., Chiaberge M., 2007, *A&A*, 466, 855
 Pietrini et al., 2014, in preparation
 Ponti G., Miniutti, G., Cappi M., Maraschi L., Fabian A. C., Iwasawa K., 2006, *MNRAS*, 368, 903
 Puccetti S., Fiore F., Risaliti G., Capalbi M., Elvis M., Nicastro F., 2007, *MNRAS*, 377, 607
 Risaliti G., 2002, *A&A*, 386, 379
 Risaliti G., 2010, *IAUS*, 267, 299
 Risaliti G., Elvis M., Fabbiano G., Baldi A., Zezas A., Salvati M., 2007, *ApJ*, 659, L111
 Risaliti G. et al., 2009, *ApJ*, 696, 160
 Risaliti G., Elvis M., Bianchi S., Matt G., 2010, *MNRAS*, 406, L20
 Risaliti G., Nardini E., Salvati M., Elvis M., Fabbiano G., Maiolino R., Pietrini P., Torricelli-Ciamponi G., 2011, *MNRAS*, 410, 1027
 Rivers E., Markowitz A., Rothschild R., 2011, *ApJS*, 193, 3
 Sanfrutos M., Miniutti G., Agis-Gonzales A., Fabian A.C., Miller J.M., Panessa F., Zoghbi A., 2013, *MNRAS*, 436, 1588
 Sobolewska M.A., Papadakis I.E., 2009, *MNRAS*, 399, 1597
 Urry C. M., Padovani P., 1995, *PASP*, 107, 803
 Ursini et al., 2014, in preparation
 Murphy D.K. and Yaqoob T., 2009, *MNRAS*, 397, 1549
 Wang J.-M., Zhang E.-P., 2007, *ApJ*, 660, 1072
 Winter L.M., Mushotzky R.F., Reynolds C.S., Tueller J., 2009, *ApJ*, 690, 1322
 Winter L.M., Mushotzky R., Lewis K., Veilleux S., Koss M., Keeney B., 2010, *AIPC*, 1248, 369
 Young M., Elvis M., Risaliti G., 2010, *ApJ*, 708, 1388
 Zhou X.-L., Zhang S.-N., Wang D.-X., Zhu L., 2010, *ApJ*, 710, 16